energies

MDPI

Article

Unshrouded Plate Fin Heat Sinks for Electronics Cooling: Validation of a Comprehensive Thermal Model and Cost Optimization in Semi-Active Configuration

Luigi Ventola [1], Gabriele Curcuruto [1], Matteo Fasano [1], Saverio Fotia [2], Vincenzo Pugliese [2], Eliodoro Chiavazzo [1] and Pietro Asinari [1,*]

[1] Energy Department, Politecnico di Torino, Corso Duca degli Abruzzi 24, 10129 Torino (TO), Italy; luigi.ventola@polito.it (L.V.); curcurutogabriele@gmail.com (G.C.); matteo.fasano@polito.it (M.F.); eliodoro.chiavazzo@polito.it (E.C.)

[2] DENSO Thermal Systems, 10046 Poirino (TO), Italy; Saverio.Fotia@denso-ts.it (S.F.); Vincenzo.Pugliese@denso-ts.it (V.P.)

* Correspondence: pietro.asinari@polito.it; Tel.: +39-011-090-4434

Academic Editor: Kamel Hooman
Received: 8 March 2016; Accepted: 27 July 2016; Published: 2 August 2016

Abstract: Plate Fin Heat Sinks (PFHS) are among the simplest and most widespread devices for electronics cooling. Because of the many design parameters to be considered, developing both cost and thermal effective PFHS is a critical issue. Here, a novel thermal model of PFHS is presented. The model has a broad field of applicability, being comprehensive of the effects of flow bypass, developing boundary layers, fin efficiency and spreading resistance. Experiments are then carried out to validate the proposed thermal model, and its good accuracy is demonstrated. Finally, an optimization methodology based on genetic algorithms is proposed for a cost-effective selection of the design parameters of PFHS, which is particularly effective with semi-active configurations. Such an optimization methodology is then tested on a commercial heat sink, resulting in a possible 53% volume reduction at fixed thermal performances.

Keywords: heat transfer enhancement; electronics cooling; plate fin heat sinks; cost optimization; genetic algorithms

1. Introduction

The progressive size reduction of electronic devices is inevitably leading to a crucial heat dissipation issue in designing novel components [1]. In fact, overheating conditions could significantly affect the performances and durability of electronic devices, eventually reducing their expected life [2]. Even though a plethora of methods have been investigated to enhance heat dissipation in the last twenty years, air cooling by means of a fan coupled with properly designed heat sinks installed on the electronic device is currently the most robust, cost-effective and commonly adopted solution for electronics cooling [3].

However, heat sinks are also finding increasing applications outside the traditional field of high-powered electronic devices. For example, heat sinks are currently applied for cooling purposes in industrial (e.g., solar applications) as well as consumer (e.g., LED) products, which are rapidly causing a change in their design and manufacture processes [4–10]. Indeed, such newer application fields are adding further requirements to the traditional structural integrity and thermal performance ones: low cost and mass production needs are leading to a substantial rethinking of the materials and processes adopted for manufacturing heat sinks.

In particular, heat sinks with plate fins are amongst the most common and studied thermal management solutions for electronic and automotive devices [11,12]. Plate fin heat sinks (PFHS) differ in manufacturing methods (stamping, extrusion, bonding, folding, additive manufacturing), type of coolant (air, liquid), material (aluminum, copper, alloys, polymeric or composite materials) and flow regime (natural, forced) [13]. Nowadays, air-cooled heat sinks manufactured by extrusion processes are the most widespread solution, being a satisfactory compromise between costs and thermal performances [13,14], both in *active* (purposely designed fan) and *semi-active* (fan already existing in the system) configurations. However, the choice of the heat sink characteristics maximizing thermal performances and minimizing production and operating costs for a particular application may be extremely complex, due to the multiple design options and restraints to be considered at the same time.

Several theoretical, numerical and experimental thermo-fluid dynamics studies on air-cooled PFHS have been carried out [15–21], in order to achieve a more fundamental understanding of the involved phenomena. More recently, the inverse method coupled with numerical simulations and experimental temperature data have been adopted to determine the average convective heat transfer coefficient in PFHS [22]; whereas a practical model for predicting the hydraulic and thermal performance of PFHS has proved accuracy within −14% to 12% for a wide range of Reynolds numbers [23]. In summary, the main phenomena to be taken into account for a comprehensive thermal model are the (1) baseplate-to-fins spreading resistance; (2) thermal conduction through fins; (3) boundary layer development along fins; and (4) flow bypass (i.e., unshrouded heat sinks) [13].

Starting from an adequate thermo-fluid model, the optimal configuration for the air-cooled PFHS can be then investigated. To this purpose, conventional thermal analysis tools are usually inadequate because both geometry and boundary conditions are not known *a priori*. Therefore, numerous optimization procedures have been proposed so far. Saini and Webb [24] adopted an analytical approach to identify the best configurations of plate-fin and plate-pin-fin heat sinks. Entropy generation minimization has been also used to optimize heat sink geometries [25], as for example reported in the studies by Culham et al. [26], Shih et al. [27] and Betchen et al. [28]. Iyengar and Bar-Cohen, instead, discussed a coefficient of performance (COP) analysis for PFHS in natural or forced convection regimes, aiming to minimize—thanks to a least-energy optimization by entropy minimization methodology—both fan pumping power and the thermodynamic work needed to manufacture and assemble the heat sink [29–32]. Furthermore, multi-objective genetic algorithms [33,34], artificial neural networks (ANNs) [35], the Kriging method associated with computational fluid dynamics [36] and integrated approaches [37] have been investigated to maximize the thermal performance of heat sinks while considering multi-constraints (e.g., pressure drop, mass, space limitations).

One of the most valid studies on this topic has been conducted by Culham et al. [38], where a thermal model for shrouded (i.e., no flow bypass) heat sinks and an optimization procedure based on entropy generation minimization have been coupled. However, optimization strategies based on entropy generation minimization only focus on operating costs, while neglecting production ones. This may lead to oversizing the heat sink, which implies an increased amount of material and thus production costs [34].

In this work, we report both a novel comprehensive thermal model and a methodological approach to designing air-cooled PFHS, which allows for optimizing the production costs at given thermal performances. First, a comprehensive thermal model suited for unshrouded heat sinks is developed, considering the effect of flow bypass, developing boundary layer along fins, heat conduction through fins and baseplate-to-fins spreading resistance. It is worth stressing that the novel thermal model has rather general validity, being easily applicable also to shrouded heat sink (no flow bypass). Second, this novel thermal model is validated by the experimental characterization of a commercial heat sink for the thermal management of an Heating, Ventilating and Air Conditioning (HVAC) control unit in the automotive field. Finally, the thermal model is coupled to an optimization procedure based on genetic algorithms, in order to find the optimal geometric parameters of PFHS in *semi-active* configurations.

This procedure is rather general, taking into account both the full range of possible working conditions and the technological constraints due to the adopted manufacturing process (e.g., extrusion and additive manufacturing). In particular, this optimization methodology is adopted to find the most cost-effective configuration for the considered commercial heat sink in a *semi-active* configuration.

The paper is structured as follows: in Section 2, the comprehensive thermal model for unshrouded heat sinks is presented; in Section 3.1, the proposed model is experimentally validated; in Section 3.2, the cost optimization methodology for heat sinks is proposed and tested; in Section 4, conclusions and perspectives are drawn.

2. Theoretical Analysis

A comprehensive model for predicting the thermo-fluid dynamics behavior of air-cooled, unshrouded PFHS under forced convection regime is introduced here.

As schematically depicted in Figure 1, the heat sink geometry considered in this work is characterized by L, H, t, and N parameters, which are the fins length, height, thickness and number, respectively. Moreover, W and t_b are the baseplate width and thickness, while p is the spacing between neighboring fins.

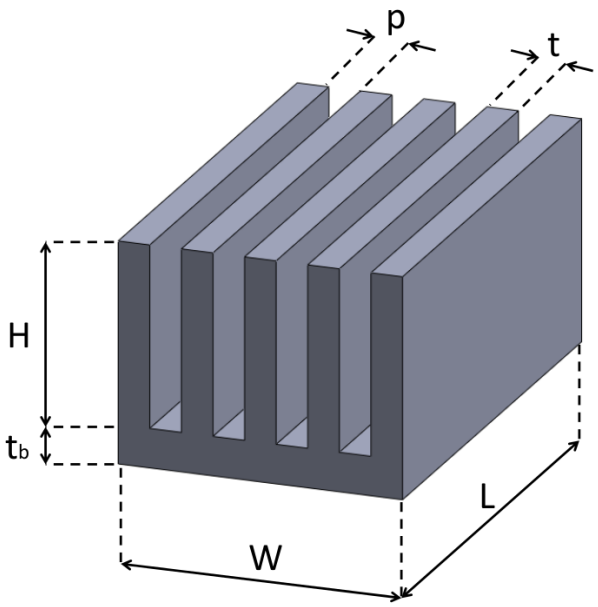

Figure 1. Heat sink geometry.

The effectiveness of heat dissipation by heat sinks depends on their effective thermal resistance, which is given by the overall effect of thermal resistances along the heat flux path, from the source to the ambient. Here, the overall junction-to-ambient thermal resistance (R_{ja}) of the electronic package is estimated relying on the classical equivalent thermal resistance network depicted in Figure 2 [13].

In fact, despite the fact that the film resistance at the fluid-solid boundary usually dominates, it has been demonstrated that the effect of other resistance elements on the heat path cannot be safely neglected in the optimization of the design characteristics of heat sinks [38].

Therefore, R_{ja} is decomposed here in four discrete components, namely:

$$R_{ja} = R_{jc} + R_{cs} + R_{sa} + R_{spr} \quad (1)$$

where R_{jc}, R_{cs}, R_{sa}, and R_{spr} are the junction-to-case, case-to-sink, sink-to-ambient, and spreading resistances, respectively.

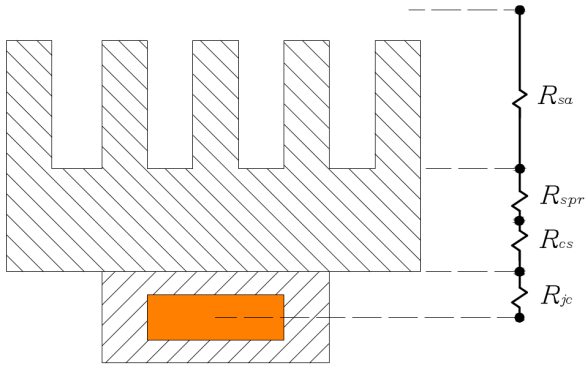

Figure 2. Scheme of the thermal resistance network of the considered heat sink.

First, in most applications, R_{jc} is given by the manufacturer, who provides the electronic components already embedded into the cases. Hence, R_{jc} is not directly modeled in the present work, being specific to the considered application and usually experimentally known.

Second, case-to-sink resistance R_{cs} is calculated as:

$$R_{cs} = \frac{t_b}{kA_b} \tag{2}$$

where k is the thermal conductivity of the heat sink, and t_b and A_b are the thickness and cross section surface area of baseplate.

Sink-to-ambient resistance R_{sa} is then computed by analytically modeling the air flow and pressure across the unshrouded heat sink. Note that the following considerations are safely applicable to any type of flow bypass (top, side or both) or to fully shrouded configurations. Figure 3 reports the average air flow velocities in the different sections of the duct where the heat sink is placed, namely: the approach velocity (v_d) at the entrance of the duct; the channel velocity (v_{ch}) through the channels made by neighboring fins (fin channels); the side bypass velocity (v_{bs}) and the top bypass velocity (v_{bt}) in the sections of the duct not occupied by the heat sink. Note that, by considering a flush-mounted installation of the heat sink on the lower wall of the duct (see Figure 3, inset), it is possible to safely approximate a 2D, laminar and fully-developed air flow through the heat sink, without longitudinal vortices.

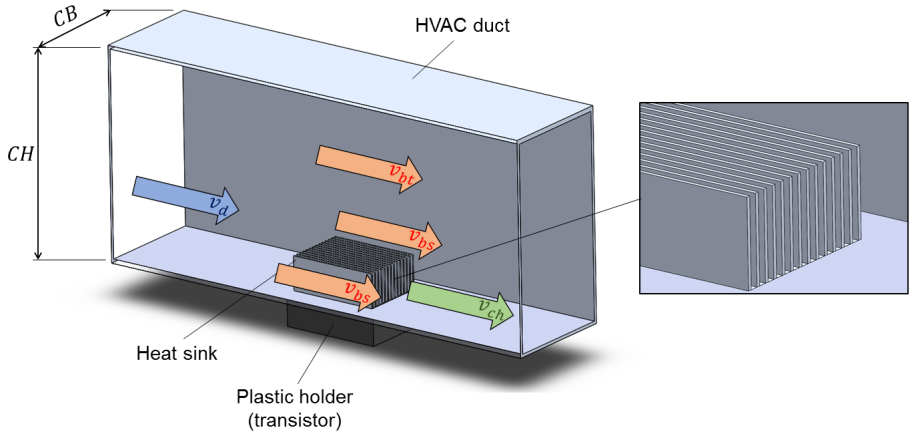

Figure 3. Scheme of the bypass phenomenon. Note that the heat sink is flush-mounted in a duct with $CB \times CH$ section, where CB and CH are channel base and height, respectively.

The air flowing through the fin channels experiences pressure drops due to contraction and expansion of the flow field at channel inlet and outlet, respectively. Let us introduce the cross section area of the duct $A_d = CB \times CH$, the overall cross section area of the fin channels $A_{ch} = (N-1)pH$, the cross section area of the side A_{bs} and the top A_{bt} bypass. Furthermore, let us assume the following conditions [39]: channel aspect ratio ($\alpha_{ch} = p/H$) less than 0.75; 2D flow through the channel of the heat sink; laminar developing flow; no air leakage from the top heat sink; uniform approach velocity; constant μ and ρ of the fluid; negligible expansion and contraction losses in the bypass sections. The air flow velocities in the different sections of the duct can be therefore obtained by applying the conservation of mass and momentum in the duct [39], namely:

$$\begin{cases} (v_{bt}^2 + v_{bs}^2) - 2v_{ch}^2 = \frac{4\Delta p_{hs} - 2(\Delta p_{bt} + \Delta p_{bs})}{\rho} \\ v_{bs}^2 - v_{bt}^2 = \frac{2(\Delta p_{bt} - \Delta p_{bs})}{\rho} \\ A_{bt}v_{bt} + A_{bs}v_{bs} = A_d v_d - A_{ch}v_{ch} \end{cases} \tag{3}$$

ρ being the air density, whereas Δp_{hs}, Δp_{bt}, Δp_{bs} are the pressure drops experienced by air flowing through fin channels, top bypass and side bypass, respectively. The complete procedure to compute Δp_{hs}, Δp_{bt} and Δp_{bs} is reported in Appendix A. By the simultaneous solution of Equations (3), the values of air velocity through the fin channels (v_{ch}), the side bypass (v_{bs}) and the top bypass (v_{bt}) can be then obtained.

Once the fluid dynamics quantities within the duct have been fully determined, it is possible to compute the modified spacing channel Reynolds $Re_p^* = Re_{ch}pL^{-1}$, where $Re_{ch} = \rho v_{ch} D_{h_{ch}} \mu^{-1}$ is the channel Reynolds number and $D_{h_{ch}} = 2p$ is the hydraulic diameter of the fin channel. The average convective heat transfer coefficient can be then calculated as:

$$h = \frac{Nu_p k_a}{p} \tag{4}$$

where k_a is the thermal conductivity of air and Nu_p is estimated as

$$Nu_p = \left[\frac{1}{\left(0.5 Re_p^* Pr\right)^3} + \frac{1}{\left(0.664\sqrt{Re_p^*} Pr^{\frac{1}{3}} \sqrt{1 + 3.65 (Re_p^*)^{-\frac{1}{2}}}\right)^3} \right]^{-\frac{1}{3}} \tag{5}$$

in the range $0.1 < Re_p^* < 100$ [40], $Pr = \mu c_{p,a}/k_a$ being the Prandtl number and $c_{p,a}$ the specific heat capacity of air at constant pressure. The fin efficiency (η) can be also determined as [40]:

$$\eta = \frac{\tanh \sqrt{2Nu_p k_a H^2 (t+L)/(kptL)}}{\sqrt{2Nu_p k_a H^2 (t+L)/(kptL)}} \tag{6}$$

The sink-to-ambient thermal resistance can be finally computed as:

$$R_{sa} = \frac{1}{\eta h A_{hs}} \tag{7}$$

A_{hs} being the total heat sink surface involved in the convective heat transfer.

The fourth thermal resistance considered in the model depicted in Figure 2 takes into account the spreading resistance between the heat source and the baseplate of heat sink. As sketched in Figure 4, spreading resistance occurs in configurations where heat flows from a small heat source to the base of a larger heat sink. In this way, the heat cannot uniformly distribute through the baseplate, therefore limiting the convective cooling effect by the fins.

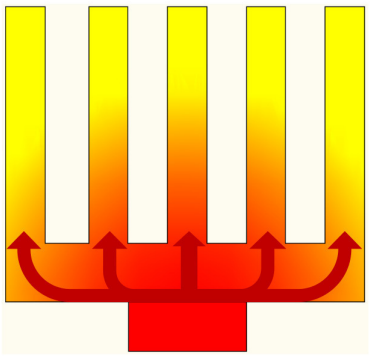

Figure 4. Scheme of heat spreading phenomenon in a PFHS: red and yellow represent high and low temperature regions, respectively; arrows represent heat propagation paths.

Spreading resistance is progressively becoming an important issue in modern microelectronics, and it can be mitigated by either increasing the thickness of the baseplate or by adopting materials with higher thermal conductivity (e.g., novel micro- and nano-structured materials [41]). Here, a perfect thermal contact between case and heat sink baseplate (i.e., negligible thermal contact resistances) is assumed, and R_{spr} is estimated following the work by Lee et al. [42], where further details are available. Let us define the baseplate and heat source (i.e., case) equivalent radii as $r_b = \sqrt{A_b/\pi}$ and $r_s = \sqrt{A_s/\pi}$, respectively, where A_s is the cross section area of the heat source.

Moreover, let us introduce the dimensionless contact radius (ϵ) and plate thickness (τ):

$$\epsilon = \frac{r_s}{r_b} \tag{8}$$

$$\tau = \frac{t_b}{r_b} \tag{9}$$

Considering the dimensionless Biot number of the baseplate as $Bi_b = hr_b/k$, it is possible to calculate the dimensionless spreading resistance $\Psi = \Psi(\epsilon, \tau, Bi_b)$ as:

$$\Psi = \frac{1}{2}(1-\epsilon)^{3/2}\frac{\tanh(\lambda\tau) + \frac{\lambda}{Bi_b}}{1 + \frac{\lambda}{Bi_b}\tanh(\lambda\tau)} \tag{10}$$

where $\lambda = \lambda(\epsilon)$ is an empirical parameter found as $\lambda = \pi + (\sqrt{\pi}\epsilon)^{-1}$ [42]. Finally, the spreading resistance R_{spr} is calculated as:

$$R_{spr} = \frac{\Psi}{k\sqrt{A_s}} \tag{11}$$

Even though the overall thermal resistance model for R_{ja} has been developed for unshrouded heat sinks, it is worth stressing that it has general validity. In fact, it can be easily applied to shrouded heat sinks by neglecting bypass phenomenon.

3. Results and Discussion

3.1. Experimental Validation

Experiments are carried out to validate the comprehensive thermal model of the heat sink discussed in Section 2. In particular, a commercially available PFHS (DENSO^{TM} Thermal Systems, Poirino (TO), Italy) is considered as a representative case study. The experimental measurements of the junction-to-ambient thermal resistance ($R_{ja,e}$) are then compared with the modeling predictions ($R_{ja,m}$), at different approach velocities (v_d) in a *semi-active*, unshrouded configuration.

The geometrical parameters of the sample heat sink experimentally tested are reported in Table 1. The considered heat sink is made out of extruded aluminum alloy (type AL EN AW 6060), and it is currently used for the heat dissipation of power transistors for the air flow control in HVAC for the vehicle passenger area.

Table 1. Geometrical parameters of the commercially available heat sink experimentally tested.

L [mm]	W [mm]	t_b [mm]	N [mm]	H [mm]	t [mm]	p [mm]
57.2	41.4	8.4	14	21.8	1	2.1

The experimental campaign has been designed to thermally characterize the heat sink in the full range of typical working conditions. During the tests, the heat sink is flush-mounted on the lower wall of the HVAC rectangular air duct (cross section area $A_d = 97.63$ cm^2, $CB = 7.47$ cm and $CH = 13.07$ cm), and it dissipates the heat generated by a power transistor. Hence, the heat sink is tested (and it usually operates) in a *semi-active* configuration, i.e., it takes advantage of an existing fan in the HVAC. The experimental rig used to characterize the heat sink is described in the following.

Air at ambient temperature enters into the rig by an inlet pipe with 150 mm diameter, where air flow rate is measured. Then, air flows into a plenum chamber with dimensions 2 m × 2 m × 1.5 m. Finally, the air flow passes through a feeding branch and enters into the HVAC. The HVAC fan is used to flow the air through the experimental rig and into the HVAC itself, where the heat sink is placed.

The transistor voltage drop (V), electric current (I), junction temperature (T_j), and temperature of air approaching heat sink (T_a) are measured by a GL220 data logger (Graphtec™ Digital Solutions, Plano, TX, USA). Type T thermocouples are used for temperature measurements: T_j is measured at the interface between transistor and heat sink base (i.e., junction-to-case, see Figure 2 and the inset in Figure 5), while T_a is measured at the HVAC inlet. Consequently, the power supplied to transistor ($P = VI$) and the overall junction-to-ambient thermal resistance $R_{ja,e} = (T_j - T_a)/P$ can be calculated.

The air flow is measured by orifice plate method. An AISI 304 steel plate (DENSO Thermal Systems) is inserted in the inlet pipe. The orifice in the plate has a diameter of 79 mm. Pressure taps are inserted upstream and downstream the plate, so that the differential pressure can be measured by a FKK differential pressure transmitter (Fuji electric™, Tokyo, Japan). By measuring differential pressure, the volumetric air flow rate ($\dot{V}$) can be easily calculated [43]. Finally, the approach velocity can be calculated as $v_d = \dot{V}/A_d$.

A schematic of the experimental rig is shown in Figure 5, while experimental results are reported in Table 2.

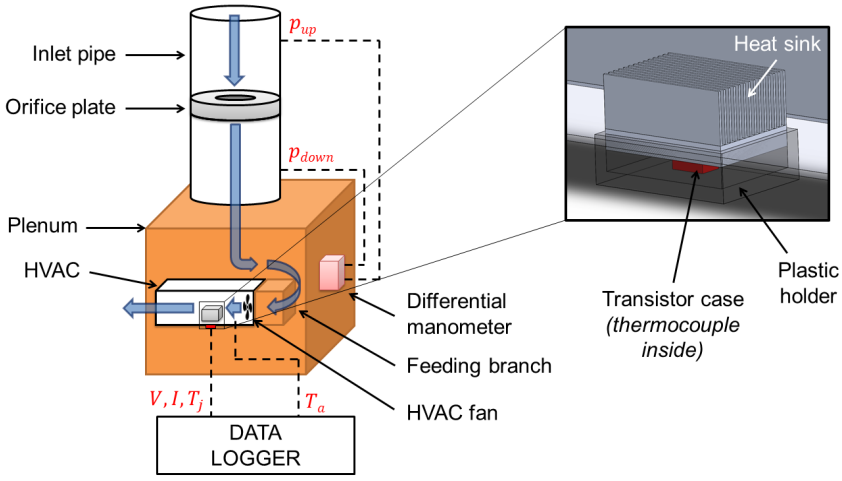

Figure 5. Scheme of experimental test rig used for heat sink characterization.

Table 2. Experimental results for the commercially available heat sink.

$\dot{V}$ [m^3/s]	P [W]	T_j [°C]	T_a [°C]	v_d [m/s]	$R_{ja,e}$ [K/W]
0.136	60.24	84.4	26.5	13.9	0.96
0.125	76.3	104.3	26.1	12.8	1.02
0.112	85.07	118	25.8	11.5	1.08
0.099	87.32	121.9	25.1	10.2	1.11
0.086	82.36	118.7	24.8	8.8	1.14
0.070	71.4	111	24.2	7.2	1.22
0.054	56.64	98.1	23.8	5.6	1.31

Modeling predictions are then obtained relying on $R_{ja,m} = R_{jc} + R_{cs} + R_{sa} + R_{spr}$, as described in Section 2. First, $R_{jc} = 0.5$ K/W is considered, as suggested by the manufacturer of the power transistor embedded into the case (model STP130NS04ZB by STMicroelectronics, Geneva, Switzerland). Second, R_{cs} is calculated from Equation (2), considering $A_b = LW = 23.68$ cm^2 and $k = 209$ W/m/K. Third, R_{sa} is calculated by means of Equations (3)–(7), considering $c_{p,a} = 1013.4$ J/kg/K, $k_a = 0.0259$ W/m/K, $\rho = 1.1794$ kg/m^3, and $\mu = 1.8415 \times 10^{-5}$ kg/m/s. It is worth mentioning that the lateral area of the baseplate is not involved in the heat transfer phenomenon because the heat sink is flush-mounted on the HVAC wall during the experiments. Consequently, the overall heat transfer area A_{hs} can be calculated as:

$$A_{hs} = WL + 2(L + t)HN \tag{12}$$

while the overall heat sink volume (V) as:

$$V = WLt_b + NtLH \tag{13}$$

Finally, R_{spr} is calculated by Equations (8)–(11), considering $A_s = 1.555$ cm^2.

Experimental results and model predictions are compared in Table 3 and Figure 6. It can be noticed that model predictions for R_{ja} values range in the narrow interval −5% to +8% (Root Mean Square (RMS) equal to 5.0%), in good agreement with the accuracy achieved by previous studies [23,40,42]. Therefore, the remarkable similarity between experimental and modeling results (Figure 6) allows for considering the thermal models presented in Section 2 as an accurate reference for optimizing the plate fins configuration, at least for the considered approach air velocities (v_d = 5.6–13.9 m/s).

Table 3. Comparison between experimental results ($R_{ja,e}$) and model predictions ($R_{ja,m}$) for the considered commercial heat sink for different values of approach velocity (v_d), with corresponding percent deviations ($\frac{R_{ja,m} - R_{ja,e}}{R_{ja,e}} \cdot 100$) between model and experiments.

v_d [m/s]	$R_{jc,m}$ [K/W]	$R_{cs,m}$ [K/W]	$R_{spr,m}$ [K/W]	$R_{sa,m}$ [K/W]	$R_{ja,m}$ [K/W]	$R_{ja,e}$ [K/W]	Deviation [%]
13.9	0.5	0.017	0.133	0.367	1.017	0.96	5.82
12.8	0.5	0.017	0.133	0.381	1.031	1.02	0.59
11.5	0.5	0.017	0.133	0.400	1.050	1.08	−3.14
10.2	0.5	0.017	0.133	0.421	1.071	1.11	−3.38
8.8	0.5	0.017	0.133	0.450	1.100	1.14	−3.57
7.2	0.5	0.017	0.133	0.492	1.142	1.22	−6.10
5.6	0.5	0.017	0.133	0.553	1.203	1.31	−8.31

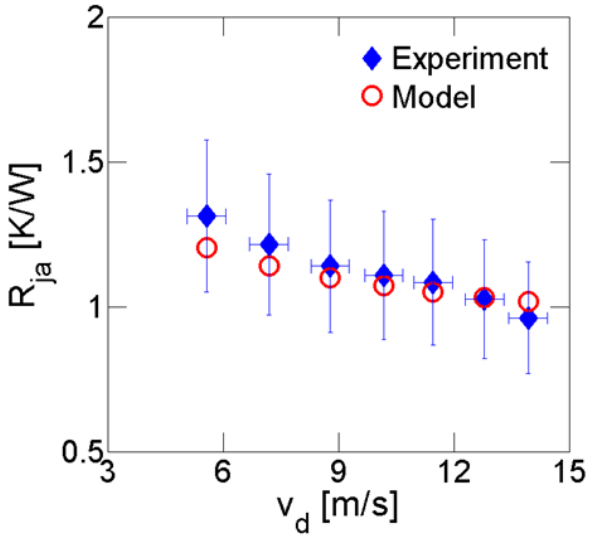

Figure 6. Comparison between experimental results and modeling predictions for the considered commercial heat sink. Experimental error bar values have been estimated relying on similar measurements [44–49]. In particular, see Appendix A in Reference [45].

The slight mismatch between modeling and experimental results may be due to both uncertainties in the v_{ch} model, which shows typical RMS between 3.9% and 8.6% [39], and to the partial dissipation of P by both radiative (from heat sink to duct walls) and conductive (through the transistor case holder) heat transfer mechanisms. As a first approximation, radiative and conductive heat transfer phenomena have been neglected in the thermal model presented in Section 2. In fact, the extruded aluminum alloy has low emissivity (≈ 0.1 [14,50]), whereas the baseplate heat sink and transistor case are mounted in a thermally insulating plastic holder.

3.2. Optimization Procedure and Results

The majority of existing approaches aim to optimize heat sink geometry to achieve the best thermo-fluid dynamics performances at the same time [13,26,38], in order to fulfill the thermal dissipation requirements with minimum operating costs (i.e., fan power, which is directly linked to pressure drops). However, the present study focuses on optimizing the material needed to manufacture a heat sink while meeting the requested thermal performances, in order to reduce production costs. This approach is particularly effective in the case of unshrouded PFHS operating in *semi-active* configurations, namely when the air flows on the heat sink thanks to an already existing fan, and thus no additional operating costs are generally involved. Here, the optimization procedure is introduced and then tested on a case study, namely the heat sink tested in Section 3.1.

Basically, the optimization algorithm takes as inputs the physical properties of air ($c_{p,a}$, k_a, ρ, μ) and heat sink (k), as well as the heat sink thermal resistances $R_{ja,W}$ to be guaranteed for different air velocities $v_{d,W}$ (i.e., working conditions). A first guess geometry should be also provided. Then, the optimization procedure finds the heat sink geometry that: (1) guarantees $R_{ja} \leq R_{ja,W}$ for each $v_{d,W}$ (i.e., the *problem constraints*); (2) guarantees a certain interval of heat sink sizes, in order to take into account manufacturing constraints; and (3) minimizes the heat sink volume V and thus the production cost. In other words, the algorithm searches for the heat sink configuration that guarantees certain thermal and manufacturing performances with the minimum amount of material. Therefore, the optimization problem has the form:

$$\min_{\mathbf{x}} V(\mathbf{x}) \quad \text{such that} \quad \begin{cases} R_{ja} \leq R_{ja,W}, & \forall v_{d,W} \\ \mathbf{LB} \leq \mathbf{x} \leq \mathbf{UB} \end{cases} \tag{14}$$

where $\mathbf{x} = (L, W, t_b, H, N, t)$ are the geometric characteristics of the heat sink to be optimized, $V = WLt_b + NtLH$ is the heat sink volume, while **LB** and **UB** are lower and upper limits for the heat sink sizes, respectively.

This optimization strategy considers the heat sink volume, i.e., the amount of material needed to manufacture the part, as the cost index. Consequently, it is suitable to deal with heat sinks manufactured by "Non Subtractive" techniques, both traditional (e.g., extrusion, casting, stamping, folding [13]) and innovative (e.g., additive manufacturing [45,46,49], carbon nanotube bundles [44]) ones.

Despite cost optimization generally meaning both production and operating cost minimization, here only production costs (i.e., heat sink volume and thus material amount) are considered for the optimization procedure. In fact, operating costs come from the power consumption of the dedicated fan, which is directly linked to the overall pressure drops of the circuit where the heat sink is placed. However, the optimization procedure suggested in this study is particularly designed for the common case of heat sinks in *semi-active* configurations, where pressure drops induced by heat sinks are usually negligible if compared with other pressure drops in the circuit. Hence, operating costs can be considered as independent from the heat sink geometry and, consequently, the cost optimization becomes a sole production cost minimization [51].

Nevertheless, it is worth stressing that the generality of the reported procedure is not affected. In fact, the optimization strategy proposed in this work can be easily adapted for operating costs by substituting V with $1/\eta_A$ ($\eta_A = \frac{Nu/Nu_{ref}}{(f/f_{ref})^{0.33}}$ is the aerothermal efficiency [45]) as the cost indicator to be minimized. In such a way, the proposed optimization methodology finds the heat sink configuration able to minimize the overall pressure drop due to the heat sink, which determines the additional fan power consumption and thus operating costs.

Considering real applications, the set of possible heat sink geometries is extremely large. Hence, an algorithm able to explore the geometry parameters space in a "smart" way is needed to find the optimal solution while spending a reasonable amount of computational time. In this study, genetic algorithms are exploited to guide the problem minimum search with a more rational generation of the heat sink geometries to be evaluated. Starting from a first guess solution given as input, the algorithm randomly generates a set of possible solutions for the problem (heat sink geometries), which is called *initial population*. For each of those possible solutions, the algorithm checks whether problem constraints are verified or not, and it evaluates the objective function. Among the solutions within the problem constraints, the algorithm chooses the ones with the smallest values of the objective function. Starting from the chosen solutions, the algorithm then generates a new population (i.e., a new set of possible solutions), relying on *crossover* and *mutation* operators. Therefore, the algorithm is designed to guide the evolution of the population toward a global, optimal solution. The population generation process is repeated until a termination condition is met, such as reaching a plateau in the objective function value or exceeding a certain number of generations. Here, the heat sink optimization problem described in Equation (14) is solved by means of the genetic minimization algorithm implemented in the MATLAB™ (MathWorks Inc., Natick, MA, USA) environment. In particular, the *ga* function is here adopted to generate successive iterations of possible heat sink geometries (see Appendix B for further details).

The thermal model defined in Section 2 and experimentally validated in Section 3.1 is used to compute R_{ja} corresponding to each generated solution and working condition. The heat sink experimentally characterized in Section 3.1 is considered as a test case for the suggested optimization strategy. The actual geometry and material parameters of the heat sink by DENSO™ Thermal Systems are adopted as first guess geometry for the genetic algorithm (see Table 1). As reported in Equation (14), we impose that the thermal resistances of the optimized solution (R_{ja}) must be equal or lower than the ones predicted for the commercial heat sink (i.e., $R_{ja,W} = R_{ja,m}$, as from Table 3), for each working condition considered (i.e., $v_{d,W} = v_d$, as from Table 3). Boundary values for the geometry parameter

are imposed in the optimization problem and reported in Table 4, being dictated by the peculiar manufacturing technique (extrusion in this case) [13].

Table 4. Lower (LB) and upper (UB) boundary values for geometry parameters of the PFHS.

Boundary type	L [mm]	W [mm]	t_b [mm]	N	H [mm]	t [mm]
LB	10	10	1	2	10	0.8
UB	100	100	10	22	50	2

Table 5 reports a comparison between the initial geometry of the commercial heat sink and the one obtained by the optimization procedure. Moreover, the baseplate (V_b), fins (V_f) and overall (V) volumes of initial and optimized heat sinks are also shown. Results show that the optimal heat sink volume is 17.6 cm^3, which is a remarkable 53% less with respect to the actual commercial heat sink volume (37.4 cm^3). Therefore, the presented optimization procedure would allow saving 19.8 cm^3 of material and thus reducing production costs, without affecting the overall thermal performances of the heat sink.

Table 5. Initial and optimized release heat sink geometries.

Configuration	L [mm]	W [mm]	t_b [mm]	N [mm]	H [mm]	t [mm]	p [mm]	V_b [cm^3]	V_f [cm^3]	V [cm^3]
Initial	57.2	41.4	8.4	14	21.8	1	2.1	19.9	17.5	37.4
Optimized	20.0	40.0	4.5	22	36.4	0.9	1.0	3.6	14.0	17.6

4. Conclusions

Given the large amount of geometric and thermo-fluid dynamics parameters strongly coupled to each other, the cost-effective selection and design of heat sinks for electronics cooling can be often a complex procedure. In this work, a novel, comprehensive thermal model of unshrouded plate fin heat sinks including (1) flow bypass; (2) developing boundary layer along fins; (3) conduction through fins (fin efficiency); and (4) baseplate to fins spreading resistance, has been developed and experimentally validated. In particular, the original combination of thermal and fluid dynamics models already reported and validated in the literature allows for basing the heat sink optimization methodology on a robust modeling framework. The experimental campaign has been carried out to characterize a commercially available plate fins heat sink, which is currently adopted for automotive applications (millions of units manufactured per year). The limited deviations between experimental results and modeling predictions allow for considering the developed thermal model as an accurate reference for optimizing the plate fins configuration.

Then, a novel approach for the cost optimization of unshrouded PFHS operating in *semi-active* configurations has been proposed. Such an approach is based on computationally efficient genetic algorithms and, as a test case, it has been adopted to optimize the geometry parameters of the commercial heat sink. The optimized heat sink configuration shows a remarkable 53% volume (i.e., production costs) decrease with respect to the commercial one, while guaranteeing the same thermal performances. For the sake of simplicity, the optimization approach has been experimentally validated only for heat sinks with plate fins and approaching velocities in the range v_d = 5.6–13.9 m/s (i.e., channel Reynolds number Re_{ch} = 528–2481); however, the procedure could be further extended to other heat sink geometries or air flow regimes.

The suggested optimization methodology has been designed for heat sinks operating in *semi-active* configurations, where the relevant cost factor is the amount of material used to manufacture the heat sink (i.e., production cost). However, we highlight that the reported procedure is rather general, being easily transferable to several thermal management solutions for electronic and automotive components.

In fact, this methodology could be scaled-up for a broad variety of: (i) heat sink geometries, e.g., with pin or flared fins; (ii) air flow regimes, e.g., with natural convection; (iii) heat sink installations, e.g., fully shrouded or top bypass ones; (iv) optimization targets, e.g., minimization of pressure drops in case of active configurations. Therefore, the industrial relevance of the methodology introduced in this article is the possible *a priori* identification of a range of optimal geometrical parameters for PFHS, according to the specific working conditions and manufacturing/performance/cost boundaries to be complied. This has the potential to drastically reduce the amount of experiments (and thus time-to-market) needed to design and characterize PFHS tailored for specific applications (i.e., "Long Tail" products), especially if coupled with additive manufacturing techniques.

Acknowledgments: The authors would like to acknowledge the NANO-BRIDGE—Heat and mass transport in NANO-structures by molecular dynamics, systematic model reduction, and non-equilibrium thermodynamics (PRIN 2012, grant number 2012LHPSJC) and the NANOSTEP — NANOfluid-Based Direct Solar absorption for Thermal Energy and Water Purification (Fondazione CRT, Torino, Italy) projects.

Author Contributions: P.A. and E.C. conceived the study; L.V., G.C. and M.F. analyzed the experiments and developed the theoretical model and the optimization algorithm; S.F. and V.P. provided the experimental data; all authors wrote the paper.

Conflicts of Interest: The authors declare no conflict of interest.

Abbreviations

The following abbreviations are used in this manuscript:

a	air
app	apparent
b	baseplate
bs	side bypass
bt	top bypass
ch	channel
d	approach
e	experimental
f	fins
hs	heat sink
j	junction
m	model
p	spacing
ref	reference
s	heat source
W	working

Appendix A: Detailed Model for Pressure Drops

First, the pressure drops experienced by air flowing through the heat sink can be formulated as [39]:

$$\Delta p_{hs} = p_c + p_f + p_e \tag{15}$$

On the one side, the contraction pressure drop is defined as:

$$p_c = K_c \left(\frac{1}{2} \rho v_d^2 \right) \tag{16}$$

K_c being correlated as:

$$K_c = 1.18 + 0.0015\sigma - 0.395\sigma^2 \tag{17}$$

for laminar flows and $\sigma = \frac{p}{p+t}$ [52]. On the other side, the expansion pressure drop can be computed as:

$$p_e = K_e \left(\frac{1}{2} \rho v_{ch}^2 \right) \tag{18}$$

K_e being correlated as:

$$K_e = 1 - 2.76\sigma + \sigma^2 \tag{19}$$

for laminar flows [52]. Furthermore, the frictional pressure drop in the channel can be estimated by the Fanning friction coefficient (f_{app}) as:

$$p_f = \frac{2 f_{app} L \rho v_{ch}^2}{D_{h_{ch}}} \tag{20}$$

where $v_{ch} = v_d/\sigma$ by conservation of mass. By considering laminar hydrodynamically developing flows and one-dimensional momentum flux of an arbitrary rectangular duct [39], the apparent friction factor is estimated by the Churchill–Usagi correlation [53], namely

$$f_{app} Re_{ch} = \left[\left(\frac{3.44}{\sqrt{L_{ch}^*}} \right)^2 + \left(\frac{24}{1 + \alpha_{ch}} \right)^2 \right]^{\frac{1}{2}} \tag{21}$$

where $L_{ch}^* = \frac{L}{Re_{ch} D_{h_{ch}}}$, $\alpha_{ch} = p/H$, $Re_{ch} = \rho v_{ch} D_{h_{ch}} \mu^{-1}$ and $D_{h_{ch}} = 2p$ with $p \ll H$.

Second, the pressure drop in the top bypass section can be formulated as:

$$\Delta p_{bt} = \frac{2 f_{app_{bt}} L \rho v_{bt}^2}{D_{h_{bt}}} \tag{22}$$

for laminar developing flows [39]. Similarly to Equation (21), the Churchill–Usagi correlation is then written as:

$$f_{app_{bt}} Re_{bt} = \left[\left(\frac{3.44}{\sqrt{L_{bt}^*}} \right)^2 + \left(\frac{24}{1 + \alpha_{bt}} \right)^2 \right]^{\frac{1}{2}} \tag{23}$$

where $L_{bt}^* = \frac{L}{Re_{bt} D_{h_{bt}}}$, $\alpha_{bt} = (CH - H)/W$, $Re_{bt} = \rho v_{bt} D_{h_{bt}} \mu^{-1}$ and $D_{h_{bt}} = \frac{2W(CH-H)}{W+(CH-H)}$.

Third, the pressure drop in the side bypass section can be formulated as:

$$\Delta p_{bs} = \frac{2 f_{app_{bs}} L \rho v_{bs}^2}{D_{h_{bs}}} \tag{24}$$

for laminar developing flows [39]. Again, the Churchill–Usagi correlation is written as:

$$f_{app_{bs}} Re_{bs} = \left[\left(\frac{3.44}{\sqrt{L_{bs}^*}} \right)^2 + \left(\frac{24}{1 + \alpha_{bs1}} \right)^2 \right]^{\frac{1}{2}} \tag{25}$$

where $L_{bs}^* = \frac{L}{Re_{bs} D_{h_{bs1}}}$, $\alpha_{bs1} = (CB - W)/2H$, $Re_{bs} = \rho v_{bs} D_{h_{bs1}} \mu^{-1}$ and $D_{h_{bs1}} = \frac{2H(CB-W)}{2H+(CB-W)}$.

Appendix B: Genetic Algorithm Settings and Performances

Genetic algorithm optimization schemes are already embedded in the MATLAB^{TM} environment by the *ga* function. Nevertheless, choosing proper settings for genetic algorithms is fundamental to achieve an optimal solution [54,55]. In particular, the *ga* settings adopted in this work are: 200 generations (maximum iteration number); 100 population size (number of solutions generated by *ga* at each iteration); 75% crossover fraction (fraction of population that is created by the crossover function at the next generation); 30% migration fraction (fraction of individuals in each subpopulation that migrates to a different subpopulation at the next generation); 10 generations between successive migration events; 10^{-14} TolFun (lower bound for the change of objective function below which optimal

solution is considered to be reached); *selectionremainder* as function to select parents of crossover and mutation children; *crossoverheuristic* as function to create crossover children; *mutationadaptfeasible* as function to produce mutation children. This optimized set of parameters has been obtained after a preliminary sensitivity study. In particular, the global minimum is generally achieved after 100 generations and with a population of at least 100 individuals. Moreover, the optimization problem is not significantly affected by the migration fraction, whereas an optimal convergence is observed at 75% crossover fraction.

References

1. Gillot, C.; Bricard, A.; Schaeffer, C. Single- and two-phase heat exchangers for power electronic components. *Int. J. Therm. Sci.* **2000**, *39*, 826–832.
2. Garimella, S.V.; Fleischer, A.; Murthy, J.Y.; Keshavarzi, A.; Prasher, R.; Patel, C.; Bhavnani, S.; Venkatasubramanian, R.; Mahajan, R.; Joshi, Y.; et al. Thermal Challenges in Next-Generation Electronic Systems. *IEEE Trans. Compon. Packag. Technol.* **2008**, *31*, 801–815.
3. Remsburg, R. *Advanced Thermal Design of Electronic Equipment*; Chapman & Hall: New York, NY, USA, 1998.
4. Khan, W.A.; Culham, J.; Yovanovich, M. The Role of Fin Geometry in Heat Sink Performance. *ASME J. Electron. Packag.* **2006**, *128*, 324–330.
5. Yeh, H.M.; Ho, C.D. Collector Efficiency in Downward-Type Internal-Recycle Solar Air Heaters with Attached Fins. *Energies* **2013**, *6*, 5130–5144.
6. Wang, G.L.; Yang, D.W.; Wang, Y.; Niu, D.; Zhao, X.L.; Ding, G.F. Heat Transfer and Friction Characteristics of the Microfluidic Heat Sink with Variously-Shaped Ribs for Chip Cooling. *Sensors* **2015**, *15*, 9547–9562.
7. Ahn, B.L.; Park, J.W.; Yoo, S.; Kim, J.; Leigh, S.B.; Jang, C.Y. Savings in Cooling Energy with a Thermal Management System for LED Lighting in Office Buildings. *Energies* **2015**, *8*, 6658–6671.
8. Jeong, M.W.; Jeon, S.W.; Kim, Y. Optimal thermal design of a horizontal fin heat sink with a modified-opening model mounted on an LED module. *Appl. Therm. Eng.* **2015**, *91*, 105–115.
9. Jeng, T.M.; Tzeng, S.C.; Yang, B.J.; Li, Y.C. Design, Manufacture and Performance Test of the Thermoelectric Generator System for Waste Heat Recovery of Engine Exhaust. *Inventions* **2016**, *1*, 2.
10. Yang, Y.T.; Tang, H.W.; Ding, W.P. Optimization design of micro-channel heat sink using nanofluid by numerical simulation coupled with genetic algorithm. *Int. Commun. Heat Mass Transf.* **2016**, *72*, 29–38.
11. Diani, A.; Mancin, S.; Zilio, C.; Rossetto, L. An assessment on air forced convection on extended surfaces: Experimental results and numerical modeling. *Int. J. Therm. Sci.* **2013**, *67*, 120–134.
12. Shaalan, R.; Saleh, A.; Mesalhy, O.; Elsayed, L. Thermo/fluid performance of a shielded heat sink. *Int. J. Therm. Sci.* **2012**, *60*, 171–181.
13. Lee, S. Optimum Design and Selection of Heat Sinks. *IEEE Trans. Compon. Packag. Manuf. Technol.* **1995**, *18*, 812–817.
14. Chen, A. Aluminum Extrusion Design and the Role it Plays in High Performance Cooling Solutions for Power Electronics. Available online: http://www.apec-conf.org/wp-content/uploads/IS3-3-1.pdf (accessed on 28 July 2016).
15. Sparrow, E.; Baliga, B.; Patankar, S. Forced convection heat transfer from a shrouded fin array with and without tip clearance. *J. Heat Transf.* **1978**, *100*, 572–579.
16. Lau, K.; Mahajan, R. Effects of Tip Clearance and Fin Density on the Performance of Heat Sinks for VLSI Packages. *IEEE Trans. Compon. Hybrids Manuf. Technol.* **1989**, *12*, 757–765.
17. Lee, R.; Huang, H.; Chen, W. A thermal characteristic study of extruded-type heat sinks in considering air flow bypass phenomenon. In Proeedings of the Sixth Annual IEEE Semiconductor Thermal and Temperature Measurement Symposium, Phoenix, AZ, USA, 6–8 February 1990; pp. 95–102.
18. Iwasaki, H.; Sasaki, T.; Ishizuka, M. Cooling performance of plate fins for multichip modules. In Proceedings of the InterSociety Conference on Thermal Phenomena in Electronic Systems, Concurrent Engineering and Thermal Phenomena, Washington, DC, USA, 4–7 May 1994; pp. 144–147.
19. Wirtz, R.A.; Chen, W.; Zhou, R. Effect of flow bypass on the performance of longitudinal fin heat sinks. *J. Electron. Packag.* **1994**, *116*, 206–211.
20. Jousson, H.; Palm, B. Thermal and hydraulic behavior of plate fin and strip fin heat sinks under varying bypass conditions. *IEEE Trans. Compon. Packag. Technol.* **2000**, *23*, 47–54.

21. Ishizuka, M.; Yokono, Y.; Biswas, D. Experimental study on the performance of a compact heat sink for LSI packages. *Proc. Inst. Mech. Eng. Part A: J. Power Energy* **2000**, *214*, 523–530.
22. Chen, H.T.; Lai, S.T.; Haung, L.Y. Investigation of heat transfer characteristics in plate-fin heat sink. *Appl. Therm. Eng.* **2013**, *50*, 352–360.
23. Wu, H.H.; Hsiao, Y.Y.; Huang, H.S.; Tang, P.H.; Chen, S.L. A practical plate-fin heat sink model. *Appl. Therm. Eng.* **2011**, *31*, 984–992.
24. Saini, M.; Webb, R.L. Heat rejection limits of air cooled plane fin heat sinks for computer cooling. *IEEE Trans. Compon. Packag. Technol.* **2003**, *26*, 71–79.
25. Bejan, A. *Entropy Generation Minimization: The Method of Thermodynamic Optimization of Finite-Size Systems and Finite-Time Processes*; CRC Press: Boca Raton, FL, USA, 1995.
26. Culham, J.; Muzychka, Y. Optimization of plate fin heat sinks using entropy generation minimization. *IEEE Trans. Compon. Packag. Technol.* **2001**, *24*, 159–165.
27. Shih, C.; Liu, G. Optimal design methodology of plate-fin heat sinks for electronic cooling using entropy generation strategy. *IEEE Trans. Compon. Packag. Technol.* **2004**, *27*, 551–559.
28. Betchen, L.J.; Straatman, A.G. A computational method for geometric optimization of enhanced heat transfer devices based upon entropy generation minimization. *Int. J. Numer. Methods Fluids* **2013**, *71*, 370–402.
29. Bar-Cohen, A.; Iyengar, M. Design and optimization of air-cooled heat sinks for sustainable development. *IEEE Trans. Compon. Packag. Technol.* **2002**, *25*, 584–591.
30. Iyengar, M.; Bar-Cohen, A. Least-energy optimization of forced convection plate-fin heat sinks. *IEEE Trans. Compon. Packag. Technol.* **2003**, *26*, 62–70.
31. Bar-Cohen, A.; Iyengar, M. Least-energy optimization of air-cooled heat sinks for sustainable development. *IEEE Trans. Compon. Packag. Technol.* **2003**, *26*, 16–25.
32. Bar-Cohen, A.; Bahadur, R.; Iyengar, M. Least-energy optimization of air-cooled heat sinks for sustainability-theory, geometry and material selection. *Energy* **2006**, *31*, 579–619.
33. Ahmadi, P.; Hajabdollahi, H.; Dincer, I. Cost and entropy generation minimization of a cross-flow plate fin heat exchanger using multi-objective genetic algorithm. *J. Heat Transf.* **2011**, *133*, 021801.
34. Chen, C.; Chen, H. Multi-objective optimization design of plate-fin heat sinks using a direction-based genetic algorithm. *J. Taiwan Inst. Chem. Eng.* **2013**, *44*, 257–265.
35. Horng, J.T.; Chang, S.F.; Wu, T.Y.; Chen, P.L.; Hung, Y.H. Thermal optimal design for plain plate-fin heat sinks by using neuro-genetic method. *IEEE Trans. Compon. Packag. Technol.* **2008**, *31*, 449–460.
36. Park, K.; Oh, P.K.; Lim, H.J. The application of the CFD and Kriging method to an optimization of heat sink. *Int. J. Heat Mass Transf.* **2006**, *49*, 3439–3447.
37. Zhou, J.; Yang, C.; Zhang, L. Minimizing the entropy generation rate of the plate-finned heat sinks using computational fluid dynamics and combined optimization. *Appl. Therm. Eng.* **2009**, *29*, 1872–1879.
38. Culham, J.; Khan, W.A.; Yovanovich, M.; Muzychka, Y. The Influence of Material Properties and Spreading Resistance in the Thermal Design of Plate Fin Heat Sinks. *J. Electron. Packag.* **2007**, *129*, 76–81.
39. Hossain, R.; Culham, J.; Yovanovich, M. Influence of Bypass on Flow Through Plate Fin Heat Sinks. In Proceedings of the 23rd IEEE Semiconductor Thermal Measurement and Management Symposium, San Jose, CA, USA, 18–22 March 2007; pp. 220–227.
40. Teertstra, P.; Yovanovich, M.; Culham, J.; Lemczyk, T. Analytical forced convection modeling of plate fin heat sinks. In Proceedings of the 15th IEEE Semiconductor Thermal Measurement and Management Symposium, San Diego, CA, USA, 9–11 March 1999; pp. 34–41.
41. Chiavazzo, E.; Asinari, P. Reconstruction and modeling of 3D percolation networks of carbon fillers in a polymer matrix. *Int. J. Therm. Sci.* **2010**, *49*, 2272–2281.
42. Lee, S.; Song, S.; Au, V.; Moran, K. Constriction-spreading resistance model for electronic packaging. *ASME/JSME Therm. Eng. Conf.* **1995**, *4*, 199–206.
43. Baker, R. *Flow Measurement Handbook: Industrial Designs, Operating Principles, Performance, and Applications*; Cambridge University Press: Cambridge, UK, 2005.
44. Shahzad, M.I.; Giorcelli, M.; Ventola, L.; Perrone, D.; Shahzad, N.; Chiavazzo, E.; Asinari, P.; Cocuzza, M.; Tagliaferro, A. Convective Heat Transfer Enhancement for Electronic Device Applications Using Patterned MWCNTs Structures. *Heat Transf. Eng.* **2016**, *37*, 783–790.

45. Ventola, L.; Robotti, F.; Dialameh, M.; Calignano, F.; Manfredi, D.; Chiavazzo, E.; Asinari, P. Rough surfaces with enhanced heat transfer for electronics cooling by direct metal laser sintering. *Int. J. Heat Mass Transf.* **2014**, *75*, 58–74.
46. Chiavazzo, E.; Ventola, L.; Calignano, F.; Manfredi, D.; Asinari, P. A sensor for direct measurement of small convective heat fluxes: Validation and application to micro-structured surfaces. *Exp. Therm. Fluid Sci.* **2014**, *55*, 42–53.
47. Ventola, L.; Scaltrito, L.; Ferrero, S.; Maccioni, G.; Chiavazzo, E.; Asinari, P. Micro-structured rough surfaces by laser etching for heat transfer enhancement on flush mounted heat sinks. *J. Phys. Conf. Ser.* **2014**, *525*, 012017.
48. Ventola, L.; Chiavazzo, E.; Calignano, F.; Manfredi, D.; Asinari, P. Heat transfer enhancement by finned heat sinks with micro-structured roughness. *J. Phys. Conf. Ser.* **2014**, *494*, 012009.
49. Ventola, L.; Dialameh, M.; Fasano, M.; Chiavazzo, E.; Asinari, P. Convective heat transfer enhancement by diamond shaped micro-protruded patterns for heat sinks: Thermal fluid dynamic investigation and novel optimization methodology. *Appl. Therm. Eng.* **2016**, *93*, 1254–1263.
50. Fang, G.; Zhou, J.; Duszczyk, J. Extrusion of 7075 aluminium alloy through double-pocket dies to manufacture a complex profile. *J. Mater. Process. Technol.* **2009**, *209*, 3050–3059.
51. DENSO Thermal Systems, Poirino (TO), Italy. Private Communication, 15 July 2015.
52. Kays, W.M.; London, A.L. *Compact Heat Exchangers*; McGraw-Hill: New York, NY, USA, 1984.
53. Churchill, S.; Usagi, R. A general expression for the correlation of rates of transfer and other phenomena. *AIChE J.* **1972**, *18*, 1121–1128.
54. Yuan, B.; Gallagher, M. A hybrid approach to parameter tuning in genetic algorithms. *IEEE Congr. Evol. Comput.* **2005**, *2*, 1096–1103.
55. Chiavazzo, E.; Fasano, M.; Asinari, P. Inference of analytical thermodynamic models for biological networks. *Phys. A Stat. Mech. Appl.* **2013**, *392*, 1122–1132.

© 2016 by the authors; licensee MDPI, Basel, Switzerland. This article is an open access article distributed under the terms and conditions of the Creative Commons Attribution (CC-BY) license (http://creativecommons.org/licenses/by/4.0/).